VOLUME 35(1992), 1, 83–88
TRIBOLOGY TRANSACTIONS

Analysis of Elastomeric O-Ring Seals in Compression Using the Finite Element Method©

ITZHAK GREEN (Member, STLE) and CAPEL ENGLISH
Georgia Institute of Technology
Atlanta, Georgia

The need for a methodology to determine the stiffness characteristics of elastomeric seals with complex geometry has prompted an investigation using a commercially available finite element code. Axial and radial compression of O-rings, as well as the influence of restraining grooves and friction, are investigated. Axisymmetric analyses are performed, and their results are compared with those obtained by other researchers who assumed plane strain conditions. The differences in the results of the axisymmetric and plane strain loading conditions increase with the level of compression, except for one loading case. The method of reduced integration is shown to effectively handle the problem of high localized hydrostatic stresses, which are especially enhanced in confined geometries, and to provide accurate results. Stiffness characteristics of O-ring seals having a range of geometric and material properties are given in a nondimensional form. This form allows for general modeling of the O-ring stiffness as a force and a spring at compression (i.e., deformation) levels up to 32 percent.

INTRODUCTION

Many mechanical systems depend upon the use of elastomeric O-rings for sealing. They are economical and effective over a broad range of service conditions and surface finishes. The stiffness and stress relationships associated with the compression of elastomeric O-ring seals have been examined by several researchers. Because elastomers are nearly incompressible, strain energy density functions were developed to describe the large elastic deformations that elastomers commonly undergo.

The earliest work in this area is that by Mooney (*1*) in his theory of large elastic deformations of isotropic materials, later complemented by Rivlin (*2*). Treloar (*3*) performed a variety of extension and compression tests which supported the theory proposed by Mooney (*1*). Rivlin (*4*) provided a summary of research in this area of continuum mechanics. Other relevant research is presented in works by Ogden (*5*), Peng and Landel (*6*), and Kao and Razgunas (*7*).

Using the theories advanced by some of the aforementioned researchers, Gent and Lindley (*8*) examined the compression characteristics of bonded rubber blocks. While this research is not directly applicable to 0-rings, Lindley (*9*) developed a simple theoretical treatment for the stiffness of laterally unrestrained toroidal rubber rings under axial compression. As the first to assume plane strain conditions, he extended his theory to obtain a force deflection relationship.

Later, Lindley (*10*), (*11*) offered a nondimensional force-deflection relationship for an O-ring.

$$\frac{F}{\pi DdE} = 1.25\delta^{3/2} + 50\delta^{6} \qquad [1]$$

F is the load, D and d are the nominal and wire diameters, respectively (see Fig. 1), E the modulus of elasticity, and δ is the compression (the axial compression divided by the wire diameter). Lindley (*10*) derived the first term analytically assuming plane strain conditions, then added the second term as an empirical correction to accommodate high compression levels (*11*). Equation [1] agreed fairly well with experimental results up to 25 percent compression.

George, Strozzi and Rich (*12*) modeled O-rings in unrestrained axial loading assuming plane strain. Their results agreed well with Lindley's predictions and experimental results by George and Williams. These will also be compared to the numerical results in this work. Dragoni and Strozzi (*13*) performed a plane strain FEM analysis of an O-ring seal restrained by a rectangular groove. The lateral walls of the groove were defined to be tangent to the undeformed O-ring, and loading was applied until the deformed O-ring filled the entire groove.

Others have measured stiffness and damping of O-ring seals in the radial mode (*14*) and in the axial-shear-twist mode (*15*), but better understanding of static properties is needed before dynamic behavior can be properly analyzed.

Presented at the 46th Annual Meeting
in Montreal, Quebec, Canada
April 29–May 2, 1991
Final manuscript approved February 13, 1991

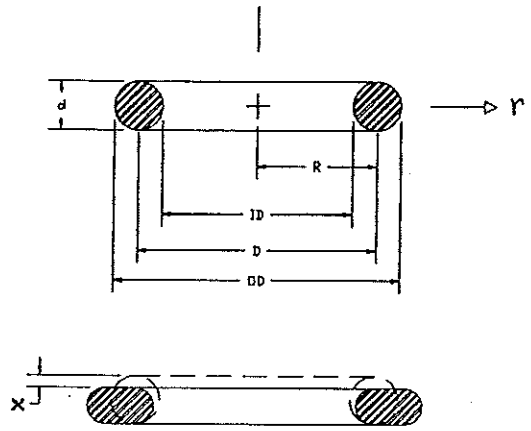

Fig. 1—Basic geometry definitions.

Elastomeric O-ring seals are typically constrained in grooves and compressed five to 25 percent. Their complex geometries and large deformations suit the finite element method. Numerical results can be verified for simple cases where experimental data is available, giving assurance of their validity for more complicated geometries.

METHOD

Five common loading conditions described in Fig. 2 (including combinations of lubricated-frictionless, unlubricated, axial, radial, restrained, and unrestrained loading) will be examined. Note that Fig. 2(b) represents two cases of axial unrestrained loading: lubricated and unlubricated. The restraining grooves are selected similarly to those in Ref. (*13*) such that the groove walls are tangent to the undeformed O-ring wire.

The major objective of this work is to determine the static stiffness characteristics of hyperelastic O-ring seals using a commercially available finite element code, (*16*). The nonlinear finite element formulation used is based upon the Mooney-Rivlin constitutive equations as implemented in element STIF84 (*16*). This allows two empirically-determined constants and a Poisson's ratio close to 0.5 to model nearly incompressible behavior.

The plan of this work is to examine the theory, to surmount its nonlinear difficulties, and to present results for axisymmetric loading. Consideration is given to mesh selection, convergence, numerical integration, and data manipulation. The methodology is applicable to other seal geometries such as X-rings or U-rings.

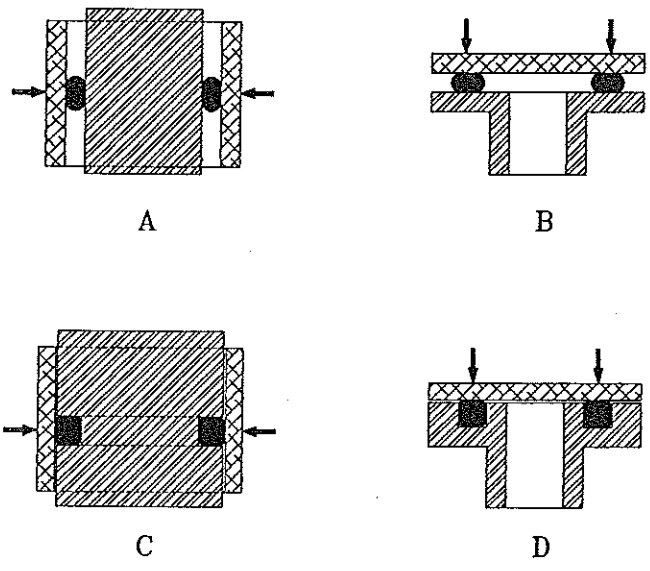

Fig. 2—(a) Unrestrained radial loading. (b) Unrestrained axial loading. (c) Restrained radial loading. (d) Restrained axial loading.

MATERIAL DESCRIPTION

A hyperelastic material can be described by a strain energy density function, W, whose derivative with respect to a strain component determines the corresponding stress component. Three principal strain invariants, I, II, and III, of the Cauchy-Green deformation tensor can be formed, see Refs. (*1*)–(*7*). While the invariants will not be defined here, they are described in terms of the principal stretch ratio, λ. If the material is isotropic, the strain energy density is a function of these strain invariants, $W = W(I,II,III)$. The Mooney-Rivlin ($M-R$) strain energy density function is the most extensively used and is implemented in the finite element code (*16*) as

$$W = A(I-3) + B(II-3) + C(1/III^2-1) + D(III - 1)^2 \quad [2]$$

Associated with this constitutive equation are four constants, A, B, C, and D, which describe a particular hyperelastic material being considered. Only A and B are independent, where C and D are functions of A and B and Poisson's ratio. As the material approaches incompressibility (i.e., $\nu = 0.5$), invariant III approaches unity leaving only the first two terms in Eq. [2]. If $B = 0$, the material is said to be neo-Hookean. The constants, A and B, describe the stress-deflection response for the type of elastomer under consideration. A is accountable for the stiffness of the material, while B precipitates a gradual increase in slope, as will be evident from the following discussion.

The principle stretch ratio, λ, is defined for uniaxial extension as

$$\lambda = \frac{l}{l_0} = \frac{l_0 + l_i}{l_0} = 1 + \frac{l_i}{l_0} = 1 + \varepsilon \quad [3]$$

where ε is the strain and l_i is the deformation. The Cauchy stress, T, is defined as the partial derivative of W with respect to the strain and is given by Kao and Razgunas (*7*) as

$$T = 2(\lambda^2 - 1/\lambda)(A + B/\lambda) \quad [4]$$

The constants A and B can be determined by curve-fitting the results from a uniaxial test to Eq. [4], and they should be non-negative (*17*). From Eq. [4] it is evident that Cauchy's stress is a nonlinear function of the stretch. A modulus of linear elasticity, E, relates to the values of the constants A and B at relatively small stretches as follows

$$\sigma = T/\lambda = E\varepsilon \quad [5]$$

Combining Eqs. [3] and [5] yields

$$T = E(\lambda^2 - \lambda) \quad [6]$$

Taking the derivative of T with respect to λ and evaluating at $\lambda = 1$ (the point where linear elasticity is assumed predominant) yields

$$\left.\frac{\partial T}{\partial \lambda}\right|_{\lambda=1} = E(2\lambda - 1)\Big|_{\lambda=1} = E \quad [7]$$

Performing the same operation on Eq. [4] results in

$$\left.\frac{\partial T}{\partial \lambda}\right|_{\lambda=1} = 6(A + B) \quad [8]$$

Hence, an expression for E as a function of A and B is obtained as

$$E = 6(A + B) = 6A(1 + B/A) \quad [9]$$

Therefore, by choosing a value for E, A can be obtained for the neo-Hookean case ($B = 0$). For $B > 0$ it is possible to vary the ratio of B/A, while maintaining a constant E, to examine non-neo-Hookean behavior.

Numerical techniques for solving finite element models of incompressible materials are complicated by the fact that Poisson's ratio, ν, is equal to or close to 0.5. The work by George et al. (*18*) provides details of modeling large strain axisymmetric and plane strain problems and describes how reduced integration allowed successful modeling of nearly incompressible materials. This method handles the numerical displacement locking that occurs most frequently where such materials are subjected to high hydrostatic stresses such as the O-ring compression cases investigated here.

NUMERICAL METHODOLOGY

Details of preprocessing (geometry and mesh generation), solution (convergence considerations), postprocessing, and data manipulation appear in English (*19*). These are summarized as follows.

Preprocessing Phase

Geometry and Mesh Generation

Because of its axial and radial symmetry, an O-ring can be modeled as axisymmetric two-dimensional (see Fig. 1). The nominal diameter, D, was held constant for all cases. To investigate the effects of curvature, the aspect ratio, d/D, was varied from one-eighth to one. Due to symmetry about the radial axis only one half of the cross-section was modeled. A two dimensional model applies also for a plane strain case; curvature, however, is immaterial.

A first order hyperelastic quadrilateral element was chosen for both the plane strain and axisymmetric problems. (See comparison by English (*19*) between first order triangular and first order quadrilateral elements.) It was also found (*19*) that doubling the mesh size to 360 quadrilateral elements caused less than two percent change at the highest compression. The results presented herein were obtained using the 360 element model.

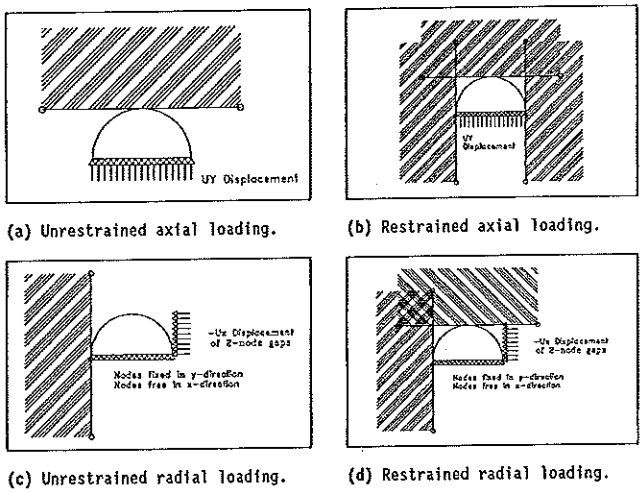

(a) Unrestrained axial loading. (b) Restrained axial loading.

(c) Unrestrained radial loading. (d) Restrained radial loading.

Fig. 3—Definition of boundary conditions and applied displacements.
(a) Unrestrained axial loading.
(b) Restrained axial loading.
(c) Unrestrained radial loading.
(d) Restrained radial loading.

Boundary Condition

Gap elements were used at contact boundaries (Fig. 3). In the case of unlubricated-unrestrained axisymmetric axial loading, a coefficient of friction of 0.9 was used to prevent slippage at the contact boundary. In all other cases frictionless gap elements were used. Ten load steps were applied to the unrestrained cases, totalling 32 percent compression. Only seven load steps were possible in restrained cases, totalling 22.4 percent compression.

Material Properties

The material was assumed homogeneous and isotropic. For the results to be normalized with respect to modulus of elasticity, 3.5 Mpa (510 psi) was chosen as typical for common rubbers. The Mooney-Rivlin constants were varied from $B/A = 0$ to 1, while maintaining E = constant (i.e., $E = 6(A+B) = 3.5$ MPa). For the majority of the cases $\nu = 0.49$ was used, but for comparison, several cases were examined with $\nu = 0.495$ and 0.499.

COMPRESSION RESULTS

The final deformations for the five loading cases of Fig. 2 are presented in Fig. 4. Dashed lines represent the undeformed geometry. As can be seen, the axial loading of the lubricated (frictionless) unrestrained O-ring causes it to translate radially. In the restrained cases the O-ring essentially fills up the groove.

Figure 5 shows a comparison of contact stress profiles at 32 percent compression for unrestrained lubricated axial loading. The reduced integration method yields much lower contact stresses (therefore, lower strain energy) suggesting more accurate results, see also examples in Ref. (*18*). All further solutions used reduced integration.

Results for normalized reaction force ($F/\pi dDE$, Fig. 6) show that varying B/A while holding E constant has very

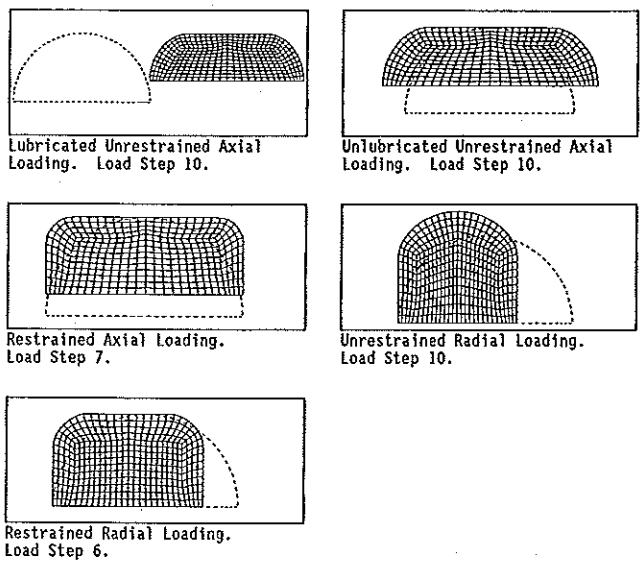

Fig. 4—Deformed *vs.* undeformed O-Ring geometries.

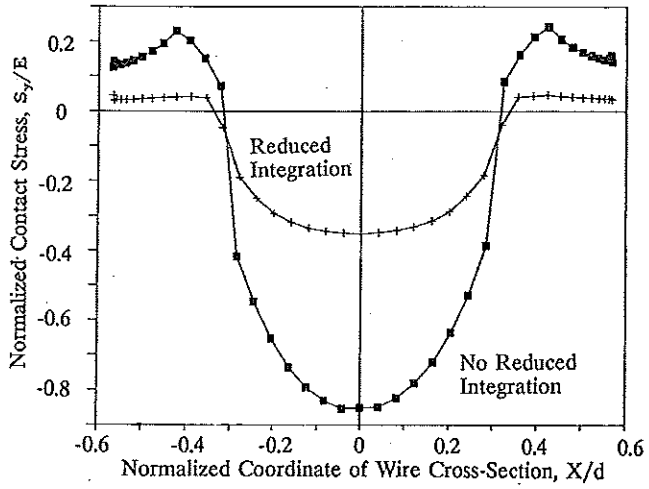

Fig. 5—Comparison of the normalized contact stress profiles at 32 percent compression.

little impact on the response. English (*19*) validated this behavior also in uniaxial loading by plotting Cauchy's stress, Eq. [4], as a function of stretch with *B/A* as a parameter. The plot shows that for deformations up to 32 percent the differences in Cauchy's stress are very small. Thus, O-rings subjected to strains up to about 30 percent can be treated as neo-Hookean.

English (*19*) found that a variation of Poisson's ratio from 0.49 to 0.495 had a negligible effect on the calculated response of all cases. However, increasing Poisson's ratio to 0.499 resulted in the divergence of the solution for restrained loadings, even at the first load step. It is suspected that the formulation in which the nearly incompressible strain energy density function is implemented in (*16*) has reached its limit. Dragoni and Strozzi (*13*) reported variation of the peak contact stress as a function of Poisson's ratio and successful application of Poisson's ratio up to 0.4999 for their code.

The effect of curvature was investigated by solving a set of axisymmetric problems where the nominal diameter remained constant at $D = 76.2$ mm (3 inches), but the diameter

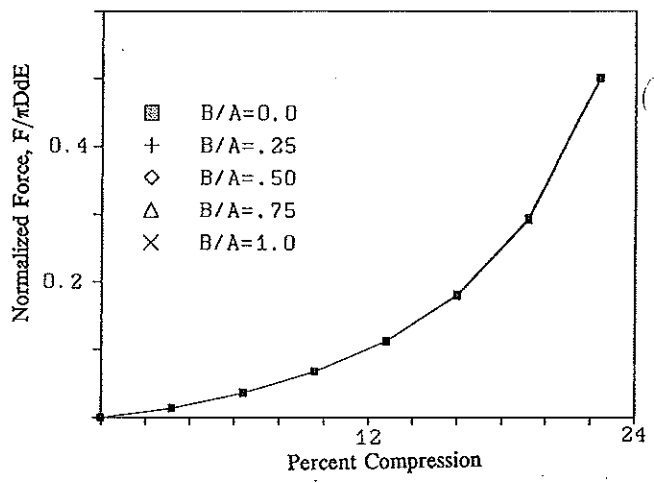

Fig. 6—The effect of various ratios of the M-R constants, *B/A*, for the case of restrained axial loading.

aspect ratio, *d/D*, varied from 1/8 to 1 in increments of 1/8. No significant differences can be detected in the results in Fig. 7 for the various aspect ratios. The experimental results in Ref. (*15*) by and large conform with this finding. For the remainder of the work here, all models use the diameter aspect ratio of 1/8, i.e., a wire diameter of 9.53 mm (0.375 inches). Since curvature has no effect on the results in axisymmetric loading, it is of interest to compare these results with those of plane strain loading. It should be pointed out that using a plane strain model implies that, because curvature is immaterial, axial and radial loading responses are indistinguishable.

The first comparison (Fig. 8) is made for all unrestrained cases, i.e. 1) lubricated-unrestrained axial loading, 2) unlubricated-unrestrained axial loading, 3) unrestrained-radial loading, and 4) unrestrained-plane strain loading. This plot clearly shows that the lubricated (frictionless) O-ring and the unlubricated O-ring (friction coefficient = 0.9) behave quite differently under axial loading conditions. The mean diameter of the well lubricated O-ring increases as the load is applied, while the cross-section becomes smaller to maintain constant volume. This case results in the lowest stiffness. The plane strain case results are similar only to

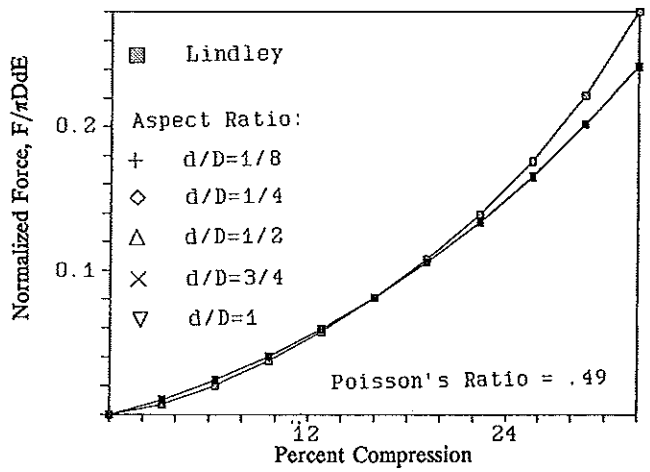

Fig. 7—The effect of various aspect ratios, *d/D*, for the case of lubricated-unrestrained axisymmetric axial compression.

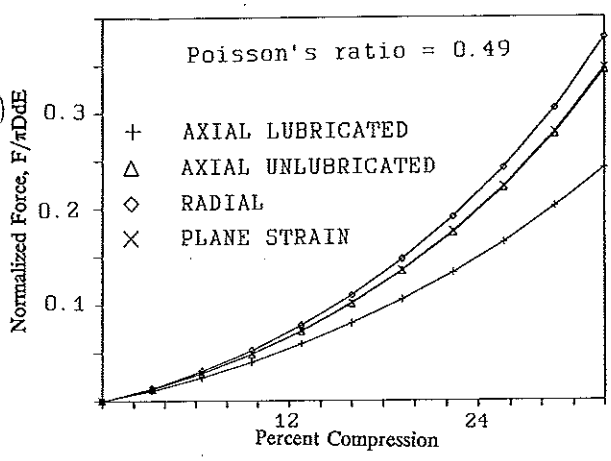

Fig. 8—Normalized force *vs.* percent compression for all unrestrained cases.

those of unlubricated axial loading, while radial loading gives the highest stiffness.

Figure 9 provides a comparison between present and previous results for the cases of unrestrained loading. These indicate that Lindley's Eq. [1] underestimates the load-deflection characteristics of all but the well lubricated O-ring. Note the good agreement of the results for unlubricated-unrestrained axial loading, and therefore, plane strain loading, with Strozzi's numerical results (Strozzi used a plane strain model). George's and Williams' experimental results also agree well with these. The good agreement of the results for these particular cases with previous work, validates the current method, and, therefore, the results for other cases. Hence, the differences between the solutions for the various cases in Fig. 9 implies that O-rings cannot always be described by the plane strain assumption for all loading cases.

Results for the three restrained cases are provided in Fig. 10. Axial, radial and plane strain results agree well up to about 10 percent compression only. As for previous cases of unrestrained loading (Figs. 8 and 9) it can be seen that the radial response is greater than either the axial response or the plane strain response. Generally, restrained loading response is greater than that of unrestrained loading.

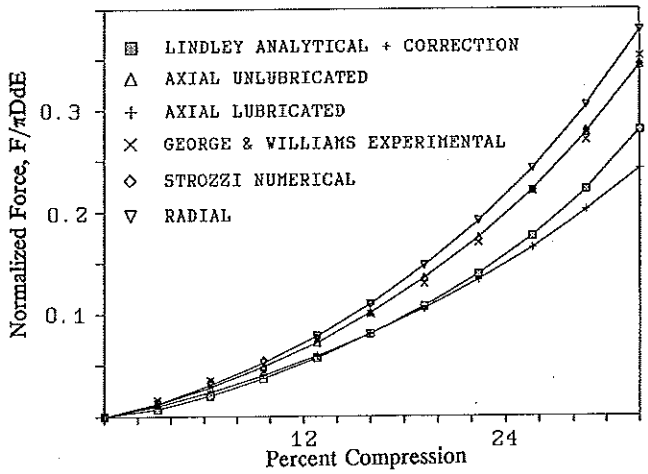

Fig. 9—Comparison with existing results for the case of unrestrained loading.

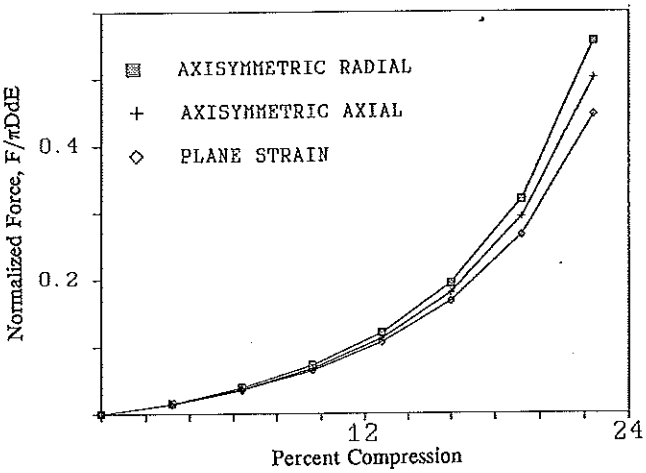

Fig. 10—Results for all three cases of restrained loading.

STIFFNESS

Expressions for nondimensional force versus compression were calculated by curve, fitting the numerical data to a two term exponential similar to Eq. [1]

$$\underline{F} = \frac{F}{\pi dDE} = a\delta^b + c\delta^d \qquad [10]$$

where $\delta = x/d$ (x being the dimensional compression). The coefficients and exponents are given in Table 1. The stiffness, K, is defined as

$$K = \frac{\partial F}{\partial x} = \frac{\partial[\pi dDE\ \underline{F}]}{\partial x} = \pi dDE\ \frac{\partial \underline{F}}{\partial x} = \pi DE\ \frac{\partial \underline{F}}{\partial \delta} \qquad [11]$$

Dimensionless stiffness is then,

$$\underline{K} = \frac{K}{\pi DE} = \frac{\partial \underline{F}}{\partial \delta} = ab\delta^{b-1} + cd\delta^{d-1} \qquad [12]$$

Hence, the dimensionless stiffness, $\underline{K}$, can be determined for all cases using the coefficients in Table 1.

SUMMARY AND CONCLUSION

Numerical analysis difficulties associated with large elastic deformation of elastomeric O-rings using a commercial finite element code have been described. No justification was found for using more terms than required by the neo-Hookean representation of material behavior. Numerical instabilities developed when Poisson's ratio approached 0.5, especially when restrained O-rings were analyzed. The method of reduced integration appears to give more realistic solutions in such cases with high localized hydrostatic stresses.

The validity of the plane strain assumption was explored, and it agreed well for the unlubricated-unrestrained axial loading case, but not as well for the other cases. It was found that the results are affected by the formulation (i.e., plane strain or axisymmetric constitutive equations), rather than by the aspect ratio or curvature. Consequently, since most

TABLE 1—LEAST-SQUARES COEFFICIENTS FOR THE CALCULATION OF NONDIMENSIONAL STIFFNESS.

TYPE OF LOADING	a	b	c	d
Axial Unrestrained Lubricated	0.74602	1.25282	3.09259	3.38757
Axial Unrestrained Unlubricated	0.97275	1.29292	6.93373	3.55385
Radial Unrestrained	1.03792	1.28710	7.77994	3.53400
Plane Strain Unrestrained	0.97184	1.29093	7.10140	3.55262
Axial Restrained	1.63328	1.38463	683.984	5.18690
Radial Restrained	1.76730	1.38755	948.475	5.32269
Plane Strain Restrained	1.55365	1.38072	530.577	5.13163

commercial codes can handle axisymmetry with the same ease as plane strain, the latter is an unnecessary assumption.

Boundary conditions were found to have a major role on the responses. This is evident from the different behaviors of lubricated *vs.* unlubricated, axial *vs.* radial, and restrained *vs.* unrestrained loadings.

Generalized analytical expressions for load-deflection, and stiffness, were presented in Eqs. [10] and [12], respectively. The coefficients in these expressions were determined by curve-fitting the numerical data for seven types of loading (Table 1).

The aforementioned expressions were made nondimensional with respect to modulus of elasticity, E. It is well known (*20*), however, that E is a function of various effects, two of which are time (relaxation) and frequency (strain rate). A proper value of E should accordingly be used for meaningful load-deflection prediction. In static loading, a relaxed value would be appropriate. In dynamic loading, E is a function of the strain rate or loading frequency, and is represented by a complex number. The real part is referenced (*20*) as the storage modulus (i.e., stiffness) and the imaginery part as the loss modulus (i.e., damping). Using the complex modulus, E, will result, respectively, in a force due to material stiffness and damping.

ACKNOWLEDGMENT

The authors gratefully acknowledge the support given to this work by the National Science Foundation REU Program under grant number MSM-8619190.

REFERENCES

(*1*) Mooney, M., "A Theory of Large Elastic Deformation," *Jour. of Appl. Phys.*, **14**, pp 582–592 (1940).

(*2*) Rivlin, R. S., "Large Elastic Deformations of Isotropic Materials. I, II, III. Fundamental Concepts," *Phil. Trans. R. Soc.*, pp 379–397, 459–490, 509–525 (1948).

(*3*) Treloar, L. R. G., "Stress-Strain Data for Vulcanized Rubber Under Various Types of Deformations," *Trans. Faraday Soc.*, **40**, (1944).

(*4*) Rivlin, R. S., "Forty Years of Continuum Mechanics," *Proc. IX Intl. Congress on Rheology, Mexico*, pp 1–29 (1984).

(*5*) Ogden, R. W., "Large Deformation Isotropic Elasticity," *Proc. Roy. Soc.*, Paper **A328** (1972).

(*6*) Peng, S. T. J. and Landel, R. F., "Stored Energy Function of Rubber-like Materials Derived from Simple Test Data," *Jour. of Appl. Phys.*, **46**, 6 (1972).

(*7*) Kao, B. G. and Razgunas, L., "On the Determination of Strain Energy Functions of Rubber, *SAE*, Paper **860816** (1986).

(*8*) Gent, A. N. and Lindley, P. B., "Internal Rupture of Bonded Rubber Cylinders in Tension," *Proc. Royal Soc.*, Series A, **249**, pp 195–205 (1959).

(*9*) Lindley, P. B., "Engineering Design with Natural Rubber," *Natural Rubber Producers Research Assoc.* Tech. Bull. **8** (1964).

(*10*) Lindley, P. B., "Load-Compression Relationships of Rubber Units," *Jour. of Strain Analysis*, **1**, pp 190–195 (1966).

(*11*) Lindley, P. B., "Compression Characteristics of Laterally Unrestrained Rubber O-Ring," *Jour. Inter. Rubber Inst.*, **1**, pp 202–213 (1967).

(*12*) George, A. F., Strozzi, A. and Rich, J. L., "Stress Fields in Compressed Unconstrained Elastomeric O-Ring seals and a Comparison with Computer Predictions with Experimental Results," *Trib. Intl.*, **20**, pp 237–247 (1987).

(*13*) Dragoni, E. and Strozzi, A., "Analysis of an Unpressurized Laterally Restrained, Elastomeric O-ring," *Trans. ASME, Jour. of Trib.*, **110**, 2, pp 193–199 (1988).

(*14*) Smalley, A. J., Darlo, M. S. and Mehta, R. K., "The Dynamic Characteristics of O-Rings," *ASME* Paper **77-DET-27** (1977).

(*15*) Green, I. and Etsion, I., "Pressure and Squeeze Effects on the Dynamic Characteristics of Elastomer O-Rings Under Small Reciprocating Motion," *Trans. ASME, Jour. of Trib.*, **108**, pp 439–445 (1986).

(*16*) DeSalvo, G. J. and Gorman, R. W., *ANSYS—Engineering Analysis System—User's Manual* (1989).

(*17*) Truesdell, C. and Noll, W., "Encyclopedia of Physics—The Non-Linear Field Theories of Mechanics," *Springer-Verlag.*, **3**, New York (1965).

(*18*) George, D., Haduch, G. A. and Jordan, S., "The Integration of Analysis and Testing for the Simulation of the Response of Hyperelastic Materials;" *Finite Elements in Analysis and Design*, **4**, pp 19–42 (1988).

(*19*) English, C., "Stiffness Determination of Elastomeric O-Rings Using the Finite Element Method," *M.S. Thesis*, Georgia Inst. of Tech. (1989).

(*20*) Nashif, A. D., Jones, D. I. G. and Henderson, J. P., *Vibration Damping*, John Wiley, New York (1985).